Available online at www.sciencedirect.com
SCIENCE DIRECT
Polymer 47 (2006) 299–309
polymer
www.elsevier.com/locate/polymer

Toughened poly(methyl methacrylate) nanocomposites by incorporating polyhedral oligomeric silsesquioxanes

Edward T. Kopesky [a], Gareth H. McKinley [b], Robert E. Cohen [a,*]

[a] Department of Chemical Engineering, Massachusetts Institute of Technology, Cambridge, MA 2139, USA
[b] Department of Mechanical Engineering, Massachusetts Institute of Technology, Cambridge, MA 2139, USA

Received 23 September 2005; received in revised form 28 October 2005; accepted 31 October 2005
Available online 21 November 2005

Abstract

We have investigated the toughenability of poly(methyl methacrylate) (PMMA) using polyhedral oligomeric silsesquioxane (POSS) nanocages at loadings between 0 and 15 wt%. Three distinct POSS species were used: a crystallizable type that did not disperse on a molecular scale within the PMMA matrix (cyclohexyl-POSS), and two types of POSS that formed homogeneous mixtures over the loadings we have investigated (methacryl-POSS and trisilanol-phenyl-POSS). Each of the three types of POSS was able to toughen PMMA in slow-speed tension tests at loadings $\leq$5 wt%; however, the reproducibility was poor due to the high flaw sensitivity of these binary blends. Ternary blends containing both cyclohexyl-POSS and methacryl-POSS showed the greatest increase in tensile toughness and also excellent reproducibility of toughening. A blend containing 2.5 wt% of both cyclohexyl-POSS and methacryl-POSS maintained the same modulus as the unfilled PMMA while increasing the toughness by a factor of 4. Electron micrographs showed extensive particle–matrix debonding of the PMMA from the cyclohexyl-POSS crystallites and some evidence of plastic deformation on the fracture surface. In high rate (1000 s^{-1}) split-Hopkinson pressure bar (SHPB) tests, binary blends of POSS and PMMA were able to improve the impact toughness of PMMA; however, once again the combined addition of both cyclohexyl-POSS and methacryl-POSS led to the greatest reproducibility of toughening. Comparison with previous results suggests that in order to toughen PMMA with rigid fillers, weakly-adhering particles with sizes on the order of 100 nm are required.

Keywords: Nanocomposies; Mechanical properies; POSS

1. Introduction

Amorphous polymers such as poly(methyl methacrylate) (PMMA), polystyrene (PS), and polycarbonate (PC) are attractive for many engineering applications because of their excellent transparencies, high moduli, and relative ease of processing. However, these polymers all exhibit shortcomings in their mechanical properties. PMMA and PS tend to be brittle materials that break at small strains when unoriented [1]. PC is usually very ductile but is highly notch-sensitive [2]. A number of studies have attempted to toughen these materials with varying degrees of success [2–10]. The challenge of concurrently increasing the toughness and the modulus of glassy polymers has proven much more difficult than doing the same in semi-crystalline polymers [11,12]. Both PMMA [8] and PS [10] have been toughened successfully with rubber particles, but high rubber contents (>30 wt%) are generally required, leading to large reductions in both the yield stress (50–75%) and the modulus (50–60%); and in most cases the optical transparency is also compromised.

The study of rubber-toughened PMMA by Jansen et al. [8] achieved superior toughness values when the average particle size in a 70:30 PMMA/rubber blend was $d=50$ nm. A recent study of PMMA filled with alumina nanoparticles by Ash et al. [4] showed a significant improvement in the tensile toughness when particles with average diameter $d=38$ nm were blended with PMMA along with the help of a methacrylic acid dispersant. The optimal particle loading was 2.2 wt%. The strain-at-break increased from $\varepsilon_{br}=0.05$ to 0.30 while the modulus and yield stress decreased by 20–25%. In addition, the glass transition temperature of the PMMA was suppressed 20 °C by the alumina nanoparticles. The use of smaller ($d=17$ nm) nanoparticles produced no improvement in toughness over the unfilled PMMA. Electron microscopy showed some evidence of deformation-induced void formation around the larger ($d=100$–200 nm) particles followed by plastic deformation of the matrix. Thus, poor interfacial adhesion between

* Corresponding author. Tel.: +1 617 253 3777; fax: +1 617 258 8224.
E-mail address: recohen@mit.edu (R.E. Cohen).

0032-3861/$ - see front matter © 2005 Elsevier Ltd. All rights reserved.
doi:10.1016/j.polymer.2005.10.143

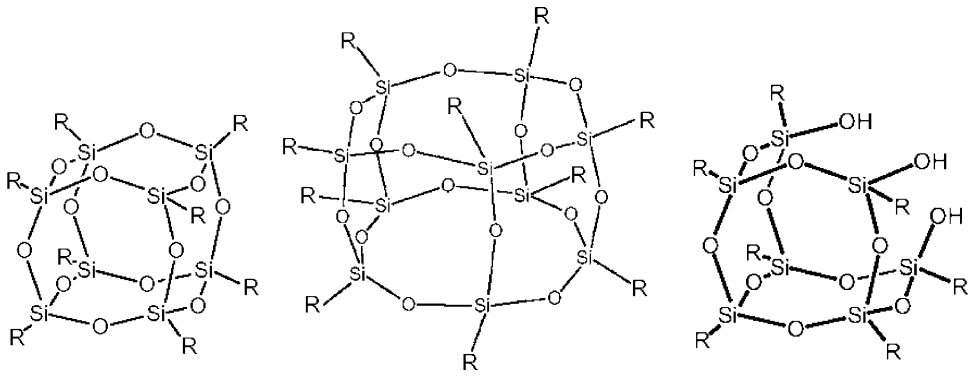

Fig. 1. (a) A T_8 POSS nanocage ($d \approx 1.5$ nm). Cyclohexyl-POSS consists of only T_8 cages and is therefore able to crystallize. (b) A T_{10} POSS nanocage. Methacryl-POSS is composed of primarily T_{10} and T_{12} cages. (c) An incompletely condensed T_8 nanocage with pendant hydroxyl groups. Trisilanol-phenyl-POSS has this cage structure.

the alumina particles and the PMMA was necessary for toughening to be observed.

In the present study, three different types of oligomeric nanocages have been blended with PMMA to observe their effect on the mechanical properties. All are polyhedral oligomeric silsesquioxanes (POSS) with the characteristic structure R_xT_x, where R represents an organic group, T represents the silsesquioxane linkage $SiO_{3/2}$, and x represents the number of silsesquioxane linkages in the cage. Representative POSS nanocages are shown in Fig. 1. One type of POSS examined in the present study, cyclohexyl-POSS, is a monodisperse, crystallizable T_8 cage (Fig. 1(a)) containing a cyclohexyl group on each corner. A previous study by us has shown that it has poor miscibility with PMMA [13] and thus phase separates into polydisperse crystallites ($50\ \text{nm} \leq d \leq 5\ \mu\text{m}$). The second POSS species, methacryl-POSS, is a polydisperse and therefore non-crystallizable POSS species composed primarily of T_{10} (Fig. 1(b)) and T_{12} cages. It is an oily liquid at room temperature and has been shown to disperse on a molecular level at loadings up to 10 wt% [14]. The final POSS species examined, trisilanol-phenyl-POSS, is an incompletely condensed T_8 cage (Fig. 1(c)) with a phenyl group on seven of the corners of the cage and the remaining corner open. This open corner contains three pendant hydroxyl groups, which have the opportunity to hydrogen-bond with the ester groups on the PMMA chains. Trisilanol-phenyl-POSS is monodisperse and therefore crystallizable yet it is extremely miscible with PMMA, completely dispersing to loadings of 20 wt%. This study aims to compare and contrast the mechanical properties of POSS-filled PMMA containing varied POSS nanocage loadings.

2. Experimental section

2.1. Materials

A commercial PMMA resin from Atofina Chemicals (Atoglas V920, $M_w = 80{,}200$ g/mol) was used as the matrix. The three different POSS species used in the study: cyclohexyl-POSS, methacryl-POSS, and trisilanol-phenyl-POSS, were all obtained from hybrid plastics (Hattiesburg, MS) and used as received.

2.2. Notes on nomenclature

Table 1 shows the nomenclature of the POSS–PMMA blends and reports their respective glass transition temperatures T_g, some of which have been reported in a previous paper [13]. The abbreviations for each type of POSS are: Cy (cyclohexyl-POSS), Acryl (methacryl-POSS), and tsP (trisilanol-phenyl-POSS).

2.3. Blending and sample preparation

Each blend was produced by dissolving first the required amount of POSS and PMMA in THF at approximately 10 wt%. The solutions were cast onto glass dishes, loosely covered with aluminum foil, and the solvent was allowed to evaporate over a period of 48 h. The films were then placed in a vacuum oven at $T = 110\ ^\circ\text{C}$ for 48 h to remove residual solvent. The dried films were then ground into a powder and processed for three minutes at $T = 225\ ^\circ\text{C}$ in a DACA instruments micro-compounder. Tensile dogbones with a

Table 1
Nomenclature and glass transition temperatures of POSS–PMMA blends

Blend name	Blend composition	T_g (°C)
PMMA	No POSS (pure PMMA)	104
2 5Acryl	2.5 wt% Methacryl-POSS	100
5Acryl	5 wt% Methacryl-POSS	97
10Acryl	10 wt% Methacryl-POSS	95
2.5Cy	2.5 wt% Cyclohexyl-POSS	104
5Cy	5 wt% Cyclohexyl-POSS	104
10Cy	10 wt% Cyclohexyl-POSS	105
2.5Cy/2.5Acryl	2.5 wt% of both cyclohexyl-POSS and methacryl-POSS	101
5Cy/5Acryl	5 wt% of both cyclohexyl-POSS and methacryl-POSS	98
5tsP	5 wt% trisilanol-phenyl-POSS	100
10tsP	10 wt% trisilanol-phenyl-POSS	99
15tsP	15 wt% trisilanol-phenyl-POSS	99

Table 2
Tensile properties of POSS–PMMA nanocomposites

Composition	Young's modulus,[1] E (GPa)	Yield stress, σ_y (MPa)	Strain-to-break ε_{br} (%)	Tensile toughness (M J/m^3)	Percent of samples yielded[2]
PMMA	2.89	67.7	6.32 (±2.81)	3.24(±1.84)	1
2.5Acryl	2.87	67.3	16.28(±15.96)	8.85(±9.04)	50
5Acryl	2.59	64.6	14.71(±9.31)	7.64(±5.11)	60
10Acryl	2.18	56.1	8.93(±3.25)	3.99(±1.73)	50
2.5Cy	2.76	63.9	13.07(±8.60)	7.03(±4.95)	67
5Cy	3.00	64.7	7.74(±3.07)	3.86(±1.87)	25
10CyP	2.58	58.6	6.27(±1.11)	2.83(±0.65)	0
2.5Cy/2.5Aceyl	2.87	61.8	25.30(±6.65)	13.29(±3.05)	100
5Cy/5Acryl	2.77	60.9	23.70(±6.65)	11.28(3.17)	90
5tsP	2.84	65.5	11.30(±6.89)	6.15(±3.84)	75
10tsP	2.93	67.5	6.80(±3.67)	3.69(±2.56)	33
15tsP	2.86	64.0	3.30(±1.70)	1.33(±0.97)	0

[a] Young's modulus measured by fitting stress–strain data between 10 and 20 MPa.
[b] A sample was determined to have yielded if it reached a strain of 8% before failure.

gauge region $20\times4.0\times1.6$ mm^3 were injected-molded from a melt kept at $T=250$ °C into a mold held at $T=60$ °C in a DACA Instruments injection molder. Split-Hopkinson pressure bar (SHPB) specimens were machined from compression-molded bars into cylinders with heights of approximately 3.5 mm and diameters of approximately 6 mm.

2.4. Characterization

A Cary 5E UV Vis-NIR dual-beam spectrophotometer was used to measure optical absorbance over the wavelength range 400 nm$\leq\lambda\leq$700 nm. Samples were thin films cast from solution with thicknesses of 50 μm.

Differential scanning calorimetry using a TA Instruments Q1000 DSC was performed to determine the glass transition temperatures T_g of the blends. The value of T_g for each blend was determined from the inflection point of the heat flow temperature curve. Samples were heated and cooled at a rate of 3 °C/min during the tests.

Scanning electron microscopy (SEM) was performed on a JEOL JSM-6060 scanning electron microscope at a voltage of 6 kV. Samples were sputter-coated with a 10 nm-thick layer of gold prior to imaging.

2.5. Mechanical tests

Tensile tests were performed on the dogbone specimens using a Zwick Z010 mechanical tester using a crosshead speed of 2 mm/min. This corresponded to an engineering strain rate of 1.7×10^{-3} s^{-1} based on the 20 mm gauge length.

Split-Hopkinson pressure bar (SHPB) tests were performed on an apparatus designed by Physics Applications, Inc. (Dayton, Ohio) [15]. For detailed background on SHPB testing see the works of Davies [16], Kolsky [17], or Gray [18]. The solid aluminum pressure bars had a length of 2.3 m and a diameter of 19.05 mm. The pressure used to create the stress wave for each test was 40 psi. The strain rate for each specimen was determined from the magnitude of the voltage of the transmitted wave as a function of time.

3. Results and discussion

3.1. Slow-speed tension tests of PMMA and POSS-filled PMMA

The stress–strain behavior of unfilled PMMA in slow-speed tension at $T=20$ °C is reported in Table 2. The modulus $E=2.89$ (±0.017) GPa and the yield stress $\sigma_y=67.7$ (±0.3) MPa remained relatively constant throughout the five samples, however the strain at break ε_{br} showed significant scatter, varying between 0.02 and 0.12. The samples showed the expected stress–strain behavior for PMMA, a fairly brittle material that is often able to reach its plastic yield point before fracture but unable to draw much further. In this section, the most ductile sample ($\varepsilon_{br}=0.12$) has been chosen as the representative curve when comparing to the POSS-filled systems in order to analyze the least-flawed samples. Reproducibility will be addressed in Section 3.3.

The PMMA was filled separately with three different types of POSS: cyclohexyl-POSS, methacryl-POSS, and trisilanol-phenyl-POSS. The degree of dispersion was, to a first approximation, estimated from the optical clarity of the material upon addition of the nanofiller. The absorbances A of these POSS-filled blend systems in the visible region (400 nm$\leq\lambda\leq$700 nm) were measured as a function of the weight fraction of POSS in each blend. Both the methacryl-POSS and the trisilanol-phenyl-POSS blends have approximately the same absorbance as PMMA up to 20 wt% loading ($A\approx0.044$), however the cyclohexyl-POSS–PMMA blends show a monotonic and substantial increase in absorbance with increased filler loading (at 10 wt% cyclohexyl-POSS, $A=0.080$).

In Fig. 2(a)–(c) we compare the stress–strain behaviors of PMMA when filled with the three different types of POSS. In Fig. 2(a) the stress–strain behavior of cyclohexyl-POSS–PMMA blends is shown for cyclohexyl-POSS loadings between 0 and 10 wt%. The cyclohexyl-POSS has little effect on the modulus but it does significantly decrease the yield stress, even at a loading of only 2.5 wt%. The strain-at-break

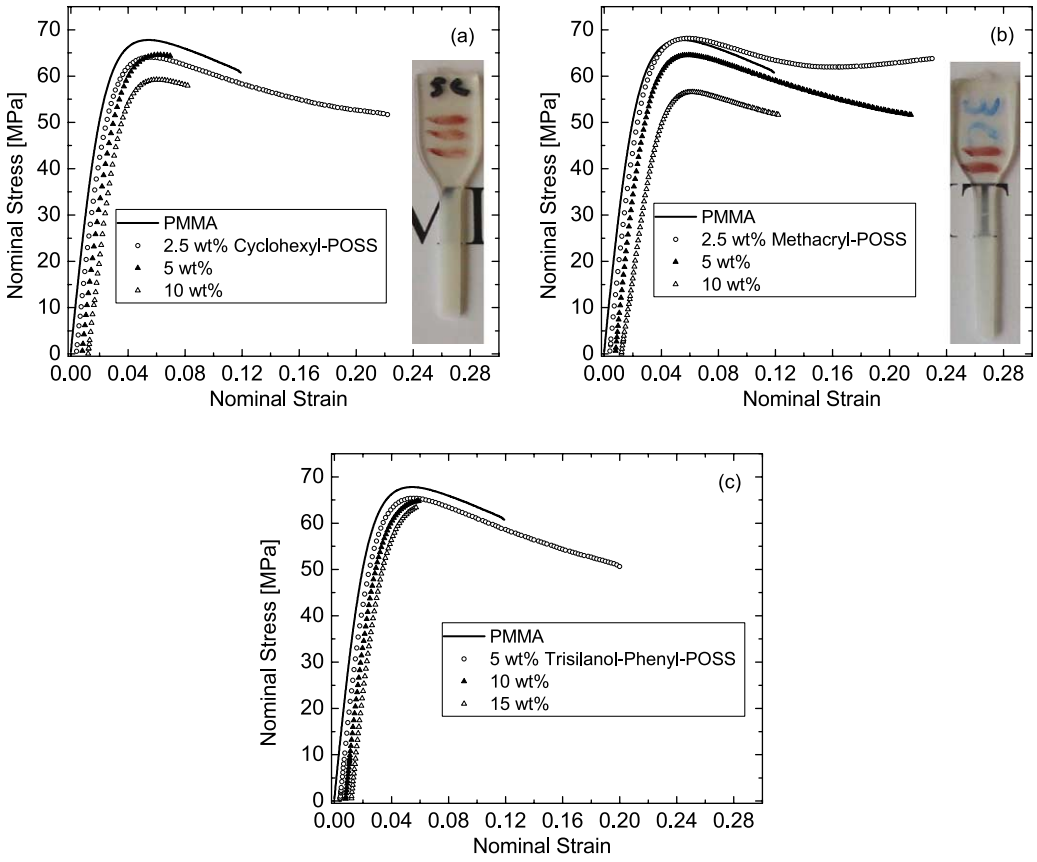

Fig. 2. Tensile properties of PMMA filled with: (a) cyclohexyl-POSS; (b) methacryl-POSS; (c) trisilanol-phenyl-POSS. The engineering strain rate was $1.7\times10^{-3}\,s^{-1}$. Curves have been offset horizontally for clarity. The picture inset in (a) is a deformed sample containing 2.5 wt% cyclohexyl-POSS that has developed haze in the gauge region after passing through its yield point. The inset to (b) is a deformed sample containing 2.5 wt% methacryl-POSS that has developed only a minor haze in the gauge region. A similar haze was observed in the more ductile samples from (c).

ε_{br} is improved significantly in the 2.5 wt% blend, nearly doubling from 0.12 to 0.23. This improvement in ε_{br} is lost at the larger loadings of 5 and 10 wt%. The more ductile cyclohexyl-POSS dogbones showed significant whitening in the gauge region during the test (see inset to Fig. 2(a)), with the onset of whitening occurring at the yield point.

In Fig. 2(b) we show the stress–strain behavior of the methacryl-POSS–PMMA blends for POSS loadings between 0 and 10 wt%. In this system, there is a noticeable decrease in the modulus at the highest loading of 10 wt%, and unlike the cyclohexyl-POSS–PMMA system, there is no decrease in the yield stress at a loading of 2.5 wt%. The softening after

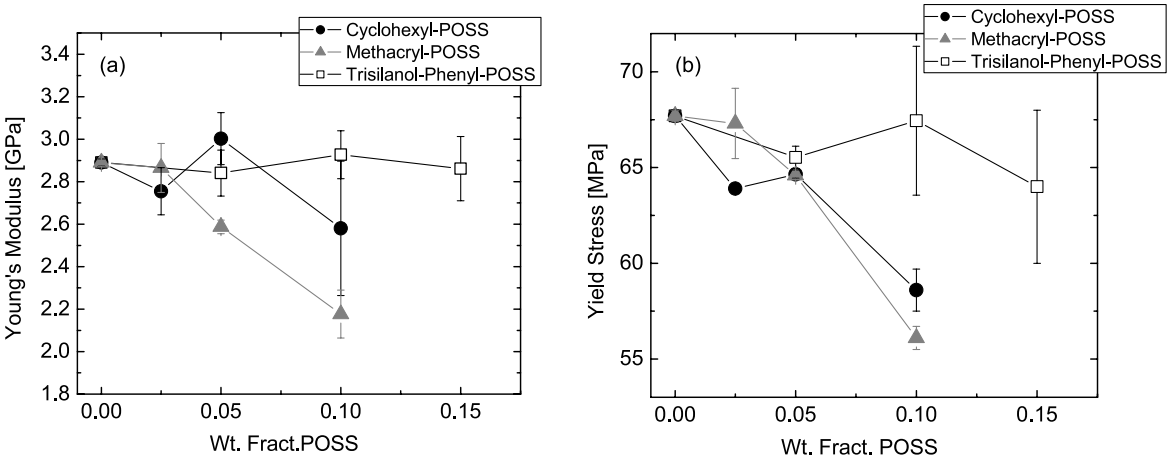

Fig. 3. Average values for (a) the Young's modulus and (b) the yield stress as a function of POSS content for PMMA filled separately with cyclohexyl-POSS, methacryl-POSS, and trisilanol-phenyl-POSS.

the yield point is also decreased at 2.5 wt% methacryl–POSS, but the degree of softening increases at 5 wt%. The strain-at-break ε_{br} increases significantly in both the 2.5 wt% and the 5 wt% blends, but at 10 wt% ε_{br} falls to less than that of the unfilled PMMA. The methacryl-POSS-filled samples, unlike the cyclohexyl-POSS-filled samples, showed no stress-whitening in the gauge region during testing. However, at loadings of 2.5 wt% and 5 wt%, the more ductile samples showed moderate haziness in the gauge region after testing (see inset to Fig. 2(b)).

In Fig. 2(c) the stress–strain behavior of the trisilanol-phenyl-POSS–PMMA blends is shown for POSS loadings between 0 and 15 wt%. As in the cyclohexyl-POSS blends, no apparent change in the modulus is observed when the POSS is added. The yield stress decreases moderately at 5 wt% but overall the decrease is much less than in the cyclohexyl-POSS and methacryl-POSS systems. The only sample to improve on the properties of the PMMA is the 5 wt% sample. No stress-whitening was observed in the trisilanol-phenyl-POSS-filled samples, only moderate haziness in the more ductile samples, similar to what was observed in the methacryl-POSS-filled blends.

All three types of POSS increase the tensile toughness of PMMA when added in very small amounts ($\leq$ 5 wt%). The cyclohexyl-POSS loses its toughening effect above 2.5 wt%, while methacryl-POSS and trisilanol-phenyl-POSS, both of which are miscible with PMMA to moderate loadings, can improve the properties of PMMA at 5 wt%. In all cases, any toughening effect is lost above 5 wt%. The relevant stress–strain properties of the blends are reported in Table 2.

In Fig. 3(a) we plot the values of the Young's modulus E for the blends as a function of POSS content. It is clear from Fig. 3(a) that at no concentration does POSS significantly increase the modulus. The Young's modulus of the methacryl-POSS–PMMA blends decreases monotonically with increasing POSS loading, with a 25% decrease at 10 wt%. The decrease, however, is negligible at the lowest loading of 2.5 wt%. The cyclohexyl-POSS-filled composites show non-monotonic changes in the modulus. The 2.5 wt% cyclohexyl-POSS–PMMA system has a slightly smaller modulus than PMMA. This is likely due to a small fraction of molecularly-dispersed cyclohexyl-POSS at this low loading. (The existence of this molecularly-dispersed component was supported by our previous rheological study of cyclohexyl-POSS–PMMA blends [13].) The modulus is slightly larger than that of PMMA at 5 wt%, due to the dominance of phase separated crystallites with relatively small diameter (d $<$ 500 nm). The modulus then becomes significantly smaller at 10 wt% as larger POSS crystallites ($d \approx 5$ μm) significantly weaken the material. The trisilanol-phenyl-POSS–PMMA system shows no significant change in modulus for loadings of 5, 10, and 15 wt%.

The effects of POSS on the yield stress σ_y of PMMA are shown in Fig. 3(b). All samples lower the yield stress, with the drop in the methacryl-POSS system being the largest. The values of the Young's modulus and the yield stress for the methacryl-POSS and the trisilanol-phenyl-POSS blends reveal the importance of the POSS R-group when the same degree of dispersion is achieved. The trisilanol-phenyl-POSS blends retain their modulus and yield stress much more than the methacryl-POSS blends, likely due to hydrogen bonding between the pendant hydroxyl groups on each trisilanol-phenyl-POSS cage and the ester groups on the PMMA chains. These multiple active sites on each nanocage prevent the trisilanol-phenyl-POSS from acting like a simple plasticizer. However, both trisilanol-phenyl-POSS and the methacryl-POSS lower the glass transition temperature of PMMA

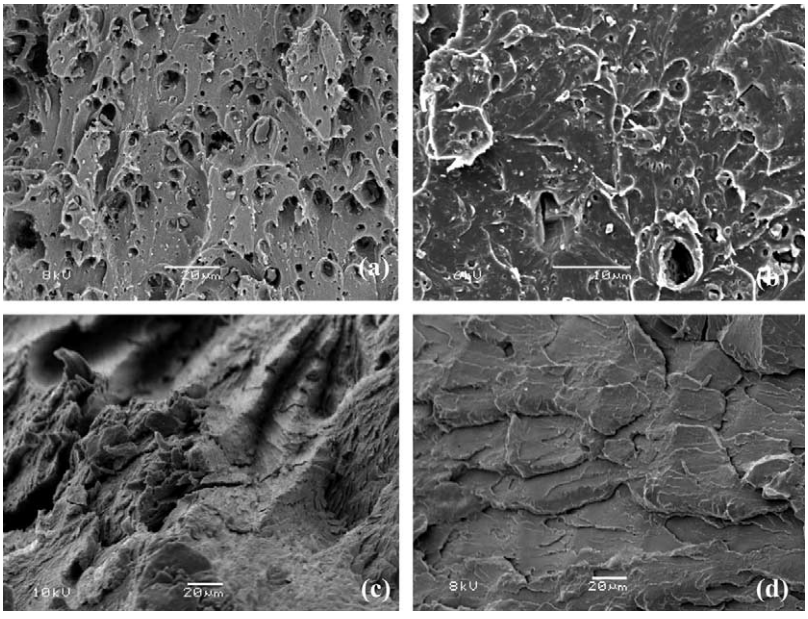

Fig. 4. SEM micrographs taken of fracture surfaces for blends containing (a) 2.5 wt% and (b) 5 wt% cyclohexyl-POSS, (c) 2.5 wt% methacryl-POSS, and (d) 5 wt% trisilanol-phenyl-POSS. The strain-at-break ε_{br} for each sample was (a) 0.23, (b) 0.05, (c) 0.22, and (d) 0.19.

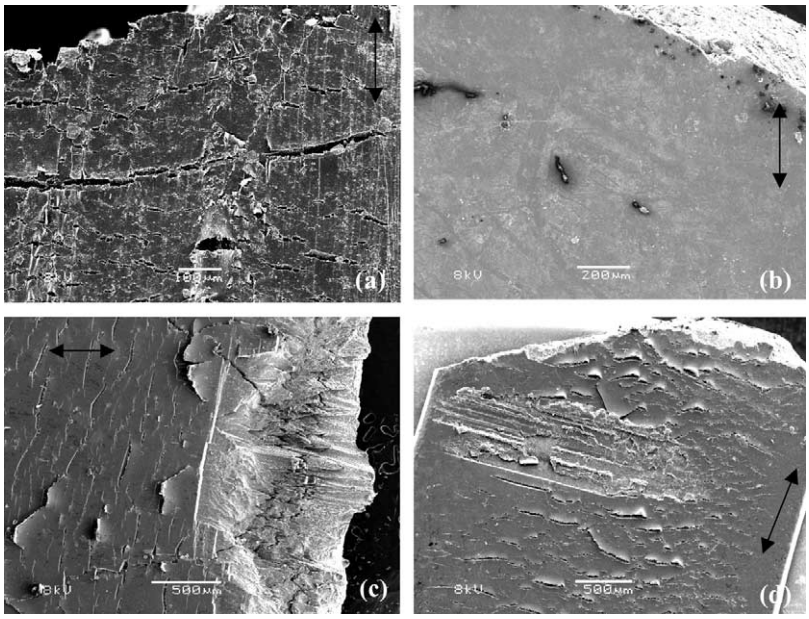

Fig. 5. SEM micrographs depicting the flat faces of tensile dogbones near the fracture surface for blends containing (a) 2.5 wt% and (b) 5 wt% cyclohexyl-POSS, (c) 2.5 wt% methacryl-POSS, and (d) 5 wt% trisilanol-phenyl-POSS. Samples (a), (c), and (d) have a similar concentration of cracks while (b), which fractured at a much lower strain, does not. The arrow on each image points in the deformation direction.

(Table 1), indicating that the improvement in tensile toughness afforded by these two species at low loadings is due to a lowering of the flow stress throughout the sample.

3.2. Scanning electron microscopy (SEM)

The scanning electron micrographs in Fig. 4 show fracture surfaces for blends containing (a) 2.5 wt% and (b) 5 wt% cyclohexyl-POSS, (c) 2.5 wt% methacryl-POSS, and (d) 5 wt% trisilanol-phenyl-POSS. In Fig. 4(a), phase separated cyclohexyl-POSS crystallites with a broad size distribution can be seen. Many small crystallites in the range $50 \leq d \leq 250$ nm are visible, and a few micron-sized crystallites are present as well. There is a high concentration of nanoscopic and microscopic voids across the sample surface, clear evidence of particle–matrix debonding during deformation. However, in Fig. 4(a) there is very little evidence of extensive drawing of matrix ligaments between particles as has been seen in particulate-filled semi-crystalline polymers [11,19]. The degree of void formation is far less significant in the 5 wt% cyclohexyl-POSS blend (Fig. 4(b)), as the sample fractured just as the debonding process began. Neither Fig. 4(c) nor (d) contains evidence of phase-separated POSS domains, consistent with molecular-level dispersion of the methacryl-POSS and the trisilanol-phenyl-POSS at these low loadings, and with the low optical absorbance values of these materials. The absence of stress-concentrating particulates in these well-dispersed blends does not allow for the particle–matrix debonding observed in Fig. 4(a); instead it appears that the plasticization caused by these dispersed POSS cages (observed in the glass transition temperatures in Table 1) causes a reduction in the flow stress, thereby allowing less-flawed samples to yield and deform.

In Fig. 5(a)–(d) we show micrographs for the same set of blends as in Fig. 4; however, these images depict the faces of the tensile dogbones near the fracture surface. In each micrograph, an arrow depicts the deformation direction. All of the samples except the 5 wt% cyclohexyl-POSS sample (Fig. 5(b)) contain a high concentration of cracks on the dogbone face that eventually led to fracture; however, the 5 wt% cyclohexyl-POSS sample did show moderate stress-whitening in the gauge region, indicating that stress-whitening is not related to surface crack formation. Therefore the only explanation for the observed stress-whitening in the cyclohexyl-POSS–PMMA blends is particle–matrix debonding at the cyclohexyl-POSS–PMMA interface. The absence of any evidence for debonding in the methacryl-POSS and the trisilanol-phenyl-POSS samples (Fig. 4(c) and (d)) leads to

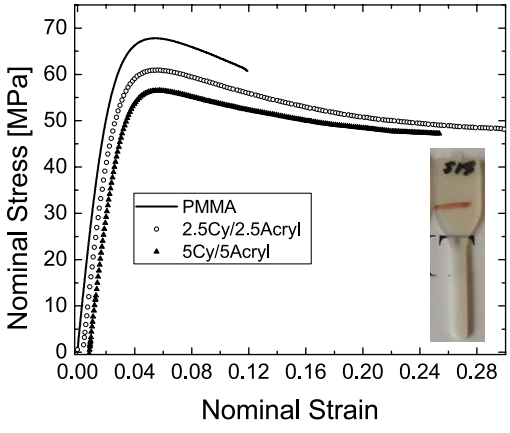

Fig. 6. Stress–strain behavior of blends containing both cyclohexyl-POSS and methacryl-POSS. Curves have been offset horizontally for clarity. The engineering strain rate was $1.7 \times 10^{-3}\ s^{-1}$. The inset shows a 5Cy/5Acryl dogbone after deformation.

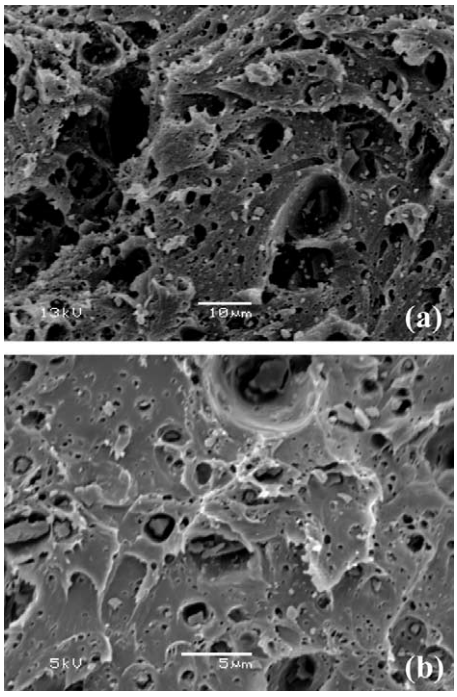

Fig. 7. Fracture surfaces for ternary blends of PMMA containing equal amounts of cyclohexyl-POSS and methacryl-POSS. The sample in (a) contained 2.5 wt% of each type of POSS and fractured at a strain $\varepsilon_{br}=0.30$. The sample in (b) contained 5 wt% of each type of POSS and fracture at $\varepsilon_{br}=0.25$.

the conclusion that the haze developed in these samples during deformation is due to the surface cracks apparent in Fig. 5(c) and (d).

The different deformation mechanisms present in the stress-whitened cyclohexyl-POSS–PMMA blends (debonding) and the methacryl-POSS blends (plasticization) suggested that the simultaneous use of these types of POSS might allow these distinct mechanisms to operate synergistically. The stress–strain behavior of PMMA blended with equal amounts of methacryl-POSS and cyclohexyl-POSS is shown in Fig. 6. The combination of these two dissimilar POSS species leads to the largest strain-at-break ε_{br} observed in any of the compositions analyzed. The blend containing 2.5 wt% of each POSS species yields and draws to a strain of $\varepsilon_{br}=0.30$. The blend with 5 wt% of each POSS species draws to a strain of $\varepsilon_{br}=0.25$. The addition of both cyclohexyl-POSS and methacryl-POSS, interestingly, causes no significant reduction in the modulus. The modulus of the 5Cy/5Acryl blend (which contains 10 wt% POSS) is 2.77 GPa, larger than both the 10 wt% methacryl-POSS blend (2.18 GPa) and the 10 wt% cyclohexyl-POSS blend (2.58 GPa), and only 4% less than PMMA (2.89 GPa).

In Fig. 7(a) and (b) we show fractures surfaces for the blends containing both cyclohexyl-POSS and methacryl-POSS. Extensive particle–matrix debonding is apparent in each case. The degree of debonding appears to be greater in the 2.5Cy/2.5Acryl blend in Fig. 7(a), which has a spongier appearance than either the 5Cy/5Acryl blend in Fig. 7(b) or the

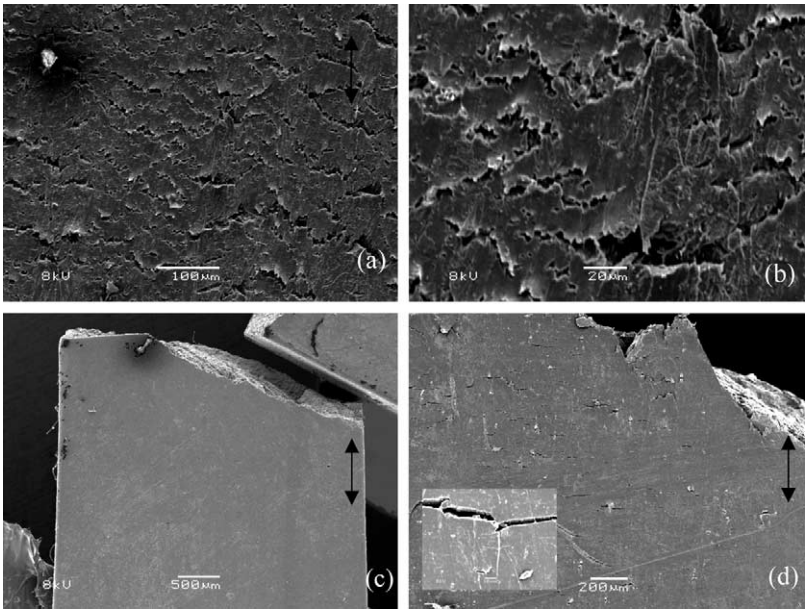

Fig. 8. SEM micrographs depicting the flat faces of tensile dogbones near the fracture surface for ternary blends containing (a), (b) 2.5 wt% of both cyclohexyl-POSS and methacryl-POSS, and (c), (d) 5 wt% of both cyclohexyl-POSS and methacryl-POSS. The arrows indicate the deformation direction. In (a) ($\varepsilon_{br}=0.30$) there is a high density of cracks, however the cracks are less sharply-defined and they appear to have difficulty propagating perpendicular to the direction of loading. In addition, a large flaw ($d=25$ μm) in the upper left-hand corner of (a) is surrounded by cracks but has not led to fracture. A closer look at the crack structure from (a) is shown in (b). Extensive plastic deformation in the matrix surrounding the cracks is apparent. No cracks are visible in (c), which fractured at a relatively low strain of $\varepsilon_{br}=0.13$. This less ductile sample did not draw into the regime where surface cracks nucleate and propagate, but instead fractured at the site of the large flaw in the upper left-hand corner. The crack structure in (d) ($\varepsilon_{br}=0.25$) is more brittle in appearance than what is observed in the less highly-filled sample from (a). The crack structure from (d) is more indicative of what is observed in Fig. 5. The inset in the lower left-hand corner of (d) shows a higher magnification of one of the cracks.

2.5 wt% cyclohexyl-POSS blend in Fig. 4(a). The PMMA matrix appears to have deformed most significantly in the 2.5Cy/2.5Acryl system, but evidence of moderate deformation of the matrix is also present in Fig. 7(b).

The flat faces of ternary dogbone samples are shown in Fig. 8(a)–(d). In Fig. 8(a) we show a side view of a sample containing 2.5 wt% of both cyclohexyl-POSS and methacryl-POSS. There is a high concentration of cracks, however the crack structure appears different from that observed in the binary samples from Fig. 5. The cracks propagate at an angle that is not normal to the deformation direction. In addition, we note that a large flaw ($d=25$ μm) is present in the upper left-hand corner of the micrograph, yet it has not caused premature fracture of the sample. A closer look at the crack structure from Fig. 8(a) is shown in Fig. 8(b). The matrix surrounding the cracks has a jagged, tooth-like appearance, with some evidence of plastic deformation of ligaments spanning the cracks. This is in contrast to the micrograph in Fig. 8(c), which shows a sample containing 5 wt% of both cyclohexyl-POSS and methacryl-POSS. This sample has failed at a lower strain of $\varepsilon_{br}=0.13$ due to a large flaw ($d=200$ μm) towards the left of the sample. No large cracks are visible on the sample surface. The adjacent image in Fig. 8(d) shows a 5Cy/5Acryl sample that deformed to a higher strain of $\varepsilon_{br}=0.25$ before fracturing. The surface of this sample contains a large number of cracks that have a more brittle structure than those in Fig. 8(a) and (b). These brittle cracks are more characteristic of those observed in the binary blends of Fig. 5. The lower left-hand corner of Fig. 8(d) shows a higher magnification look at one of the cracks on the 5Cy/5Acryl sample surface. It contains none of the jagged appearance of the cracks in Fig. 8(a) and (b).

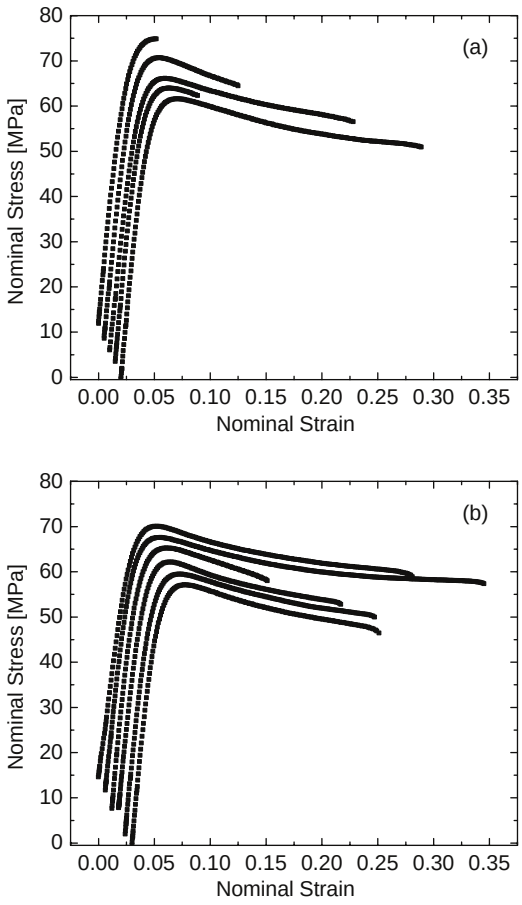

Fig. 9. Stress–strain properties of (a) 5 wt% methacryl-POSS in PMMA; (b) 5 wt% methacryl-POSS and 5 wt% cyclohexyl-POSS in PMMA. Curves have been offset both vertically and horizontally for clarity.

3.3. Reproducibility of stress–strain results

While six blend compositions plotted in Figs. 2 and 6 had the ability to improve the tensile toughness of PMMA, these compositions showed widely variable degrees of reproducibility. In Fig. 9(a) and (b) we show the entire set of tensile stress–strain curves for the 5 wt% methacryl-POSS-filled samples and six of the 5 wt% cyclohexyl/5 wt% methacryl-POSS-filled samples, respectively. The samples containing only methacryl-POSS (Fig. 9(a)) show a widely varying degree of elongation. Two samples draw beyond a strain of $\varepsilon=0.20$ while two samples fail at a strain of less than $\varepsilon=0.06$. Therefore while the tensile toughness of 7.64 M J/m^3 reported in Table 2 for the 5Acryl sample set is on average more than double that of PMMA, it has a standard deviation (5.11 M J/m^3) that is two-thirds of the average value.

In Fig. 9(b), however, it is clear that the combination of both methacryl and cyclohexyl-POSS leads to excellent reproducibility. All samples were able to yield before breaking and only one sample out of six failed before reaching a strain of $\varepsilon=0.20$. The average tensile toughness increases by a factor of 3.5 over PMMA with a standard deviation that is only 28% of the average value (Table 2). Most significant is the fact that over 90 percent of the samples containing both cyclohexyl-POSS and methacryl-POSS (2.5Cy/2.5Acryl and 5Cy/5Acryl) yielded before fracture. These ternary blends showed the best properties: retaining the modulus, increasing the tensile toughness, and reducing the flaw sensitivity of the PMMA. The reduced flaw sensitivity is most apparent in the 2.5Cy/2.5Acryl blends, which showed a noticeably different crack structure from all of the other compositions analyzed (Fig. 8(a) and (b)).

3.4. Effect of an adhesion-promoting polymer

To investigate further the role of interfacial adhesion between particles and matrix, additional tests were performed on the cyclohexyl-POSS system using an adhesion-promoting polymer. A sample containing 5 wt% cyclohexyl-POSS in PMMA was blended with a PMMA copolymer containing 15 wt% cyclohexyl-POSS tethered to the chain. The copolymer constituted 10 wt% of the blend. This well-entangled copolymer ($M_w\approx250{,}000$ g/mol) was added with the expectation that it would preferentially migrate to the interface between the cyclohexyl-POSS crystallites and the PMMA matrix and suppress debonding. The stress–strain behavior of this blend, compared with the 5 wt% cyclohexyl-POSS blend, is shown in Fig. 10(a). While the 5 wt% cyclohexyl-POSS samples could often reach their yield point before fracturing, the blends

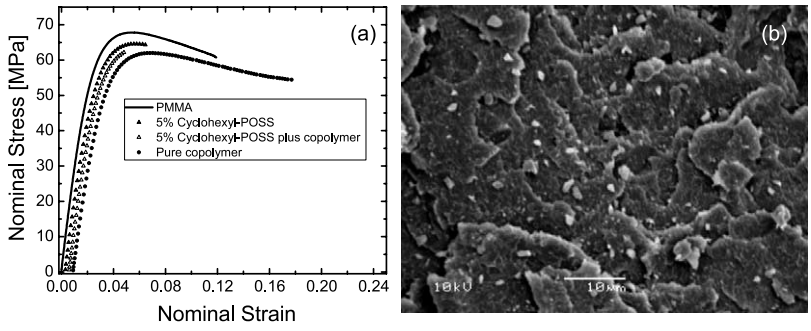

Fig. 10. (a) Tensile stress–strain curves comparing a 5 wt% cyclohexyl-POSS blend with a 5 wt% cyclohexyl-POSS blend containing 10 wt% of a cyclohexyl-POSS–PMMA copolymer to improve adhesion between POSS particles and the matrix. In addition, the stress–strain behavior of the PMMA and the pure copolymer have been plotted. The curves are offset by a strain $\Delta\varepsilon = 0.003$ for clarity. (b) Fracture surface of a 5 wt% cyclohexyl-POSS blend containing 10 wt% cyclohexyl-POSS–PMMA copolymer. No voids are present, indicative of a strong particle–matrix bond facilitated by the copolymer.

containing the adhesion-promoting copolymer were unable to reach a yield point and fractured before any stress-whitening could be observed. The micrograph in Fig. 10(b) shows that no voids have formed around the cyclohexyl-POSS particles. The complete absence of voids in Fig. 10(b) is a signature of strong adhesion between the particles and the matrix. These observations demonstrate the importance of proper interfacial interactions when rigid particles are used as toughening agents. Strong adhesion prevents matrix debonding at moderate levels of stress, precluding the formation of voids and subsequent matrix deformation. Thus the strong particle–matrix bond afforded by the copolymer is detrimental in our blends; it reduces the toughness significantly and yields no improvement to the Young's modulus.

3.5. Split-Hopkinson pressure bar (SHPB) tests

In addition to the slow-speed tension experiments, high-rate tests were performed using a Split-Hopkinson pressure bar (SHPB) apparatus. Four compositions were investigated: unfilled PMMA, 5 wt% cyclohexyl-POSS, 5 wt% methacryl-POSS, and 5 wt% of both cyclohexyl-POSS and methacryl-POSS. The stress–strain results from the SHPB tests are shown in Fig. 11(a) and (b). The stress–strain curves in Fig. 11(a) show that the PMMA did not pass through its yield process before fracturing in the compressive Hopkinson bar test. The peak stress of 305 MPa is close to the yield stress of PMMA reported by Mulliken and Boyce [$\sigma_y = 301$ MPa at a rate of 800 s^{-1}] using the same apparatus [15]. In that previous study, the PMMA was able to yield but it fractured at a strain $\varepsilon \approx 0.15$. All of the PMMA samples in this study were destroyed by the test, leaving behind only small, shredded fragments.

The POSS-filled samples, however, all deformed well past the yield point without fracturing. These samples exhibited reduced values of the yield stress in varying amounts (see inset to Fig. 11(a)). Fig. 11(b) shows a plot of strain rate as a function of strain for each of the samples tested. As the plot shows, the strain rate is not constant in the Hopkinson bar test, but for all the samples the average strain rate was centered about 1000 s^{-1}.

The average impact energy from the SHPB tests is plotted in Fig. 12 for each sample set. The average impact energy for PMMA is the smallest (20.6 ± 4.4 M J/m^3). The blends containing 5 wt% cyclohexyl-POSS exhibited a significantly higher average impact energy (36.7 ± 22.0 M J/m^3), however three of the five samples fractured near the yield point, causing the large uncertainty. Similar uncertainty was observed in the

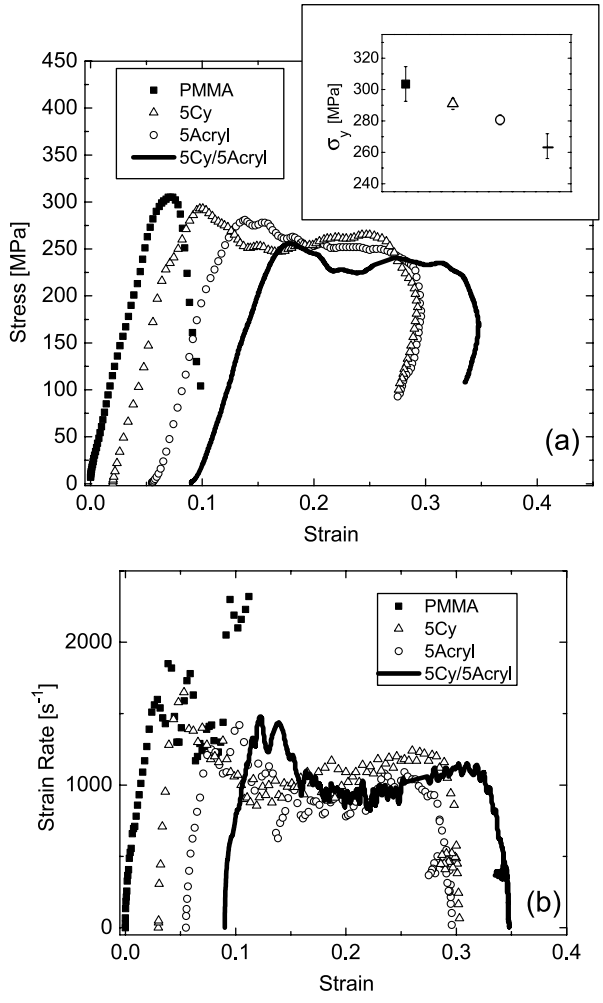

Fig. 11. (a) Split-Hopkinson pressure bar stress–strain data for PMMA and POSS–PMMA blends. Curves have been offset by a strain of 0.03 for clarity. The inset is a plot of the average yield stress for the four different sample sets tested. (b) Strain rate as a function of true strain in split-Hopkinson pressure bar Tests. Curves have been offset by a strain of 0.03 for clarity.

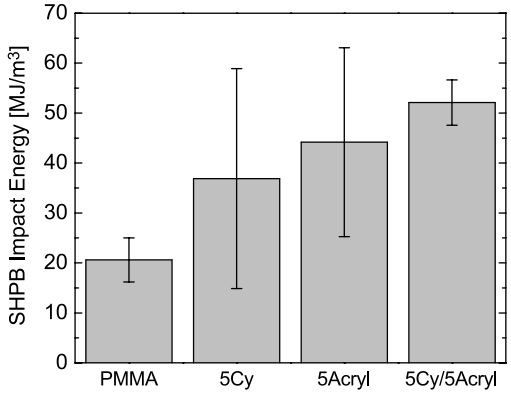

Fig. 12. Average impact energies for split-Hopkinson pressure bar (SHPB) tests on POSS–PMMA blends.

5 wt% methacryl-POSS blends (44.2 ± 18.9 M J/m^3), though only one of four samples fractured prematurely. Only in the ternary blend system containing 5 wt% of both cyclohexyl-POSS and methacryl-POSS was complete reproducibility of the yielding observed (52.1 ± 4.5 M J/m^3). All five of the 5Cy/5Acryl samples that were tested yielded and deformed without being destroyed by the impact event.

In Fig. 13, we show low magnification scanning electron micrographs for the 5Cy, 5Acryl, and 5Cy/5Acryl SHPB samples after testing. The samples all look similar in appearance, with a large number of cracks having propagated through the samples as a result of the impact event. Through the cracking and attendant local plastic deformation, the samples were able to absorb the high-rate energy impact without completely rupturing. Note that the enlarged specimen diameters ($d_0 = 3.5$ mm) are clear evidence of the permanent plastic deformation that has been achieved in these high-rate compressive tests.

4. Discussion

The greatest degree of toughening in tensile tests was observed when particle–matrix debonding occurred near the yield point. In order for the debonding to occur, particulate heterogeneities were required (Section 3.2) along with a weak interfacial bond between the particles and the matrix (Section 3.4). No debonding was observed in the methacryl-POSS–PMMA blends or the trisilanol-phenyl-POSS–PMMA blends because in each case the POSS was molecularly-dispersed. In the cyclohexyl-POSS–PMMA blends, debonding was observed at 2.5 wt% cyclohexyl-POSS; however, poor reproducibility was observed and, as the micrograph in Fig. 4(a) shows, the fracture surface appears more brittle than that observed in the ternary blend of Fig. 7(a), which contains 2.5 wt% of both cyclohexyl-POSS and methacryl-POSS. As Fig. 8(a) and (b) suggest, the improved reproducibility in the Cy/Acryl blends can be ascribed largely to the larger amount of plastic deformation needed to develop the partially-bridged crack structure that is characteristic of these blends (Fig. 8(b)). This leads to the reduced flaw sensitivities of these samples. Brittle crack formation is suppressed in the 2.5Cy/2.5Acryl system, thus allowing these samples to draw reproducibly to strains of $\varepsilon > 0.25$. The 5Cy/5Acryl blends also showed improved reproducibility in both tensile tests and split-Hopkinson pressure bar tests, however their slightly lower tensile toughness than the 2.5Cy/2.5Acryl blends can be ascribed to the higher concentration of micron-sized crystallite inclusions of cyclohexyl-POSS which lead to fracture.

The toughening observed in our POSS–PMMA blends is qualitatively similar to the results of Ash et al. [4] for PMMA filled with alumina nanoparticles. In both studies, a weak interfacial bond was necessary to observe toughening, and, in both cases, strengthening of the interfacial bond (which we accomplished by incorporating a copolymer of cyclohexyl-POSS and PMMA (Fig. 10)) led to embrittlement of the samples. The study of Ash et al. and also the rubber-toughening study of Jansen et al. [8] observed enhanced toughening when inclusions with sizes of approximately 50 nm were used. In our cyclohexyl-POSS system, the particle size distribution is broad but a large number of crystallites in the range $50\ \text{nm} \leq d \leq 200\ \text{nm}$ are present and participate in the debonding process. Thus it seems a general result for PMMA is that inclusions of approximately 100 nm that have a weak affinity for the matrix tend to toughen it in the absence of supercritical flaws; a third component, such as methacryl-POSS in our case or methacrylic-acid in the case of Ash et al.[4], can be added to make the samples less flaw-sensitive. In our study, the 2.5Cy/2.5Acryl blends achieved reproducible toughening while maintaining the modulus of the unfilled PMMA, a result superior to the studies of Ash et al. [4] and Jansen et al. [8], where substantial reductions in the modulus were seen. Future studies on PMMA nanocomposites with a narrower particle size distribution ($d \approx 100$ nm) to minimize flaws would be useful. An added benefit from samples containing smaller nanoparticles would be their higher optical clarity than the cyclohexyl-POSS nanocomposites analyzed in this study.

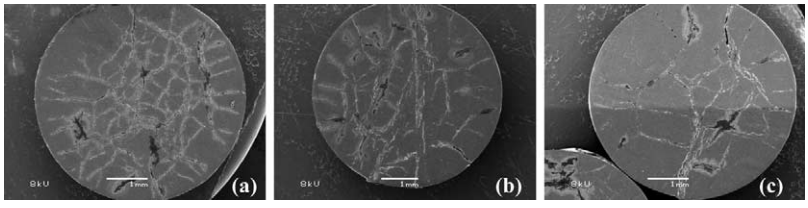

Fig. 13. Split-Hopkinson pressure bar specimens after testing: (a) 5 wt% cyclohexyl-POSS; (b) 5 wt% methacryl-POSS; (c) 5 wt% of both cyclohexyl-POSS and methacryl-POSS. The white bar represents 1 mm in each case.

5. Conclusion

In both slow-speed tension (strain rate $= 0.0033\ s^{-1}$) and high-rate split Hopkinson pressure bar tests (strain rate $= 1000\ s^{-1}$), polyhedral oligomeric silsesquioxanes(POSS) toughened PMMA by up to a factor of 4. Three types of POSS were examined: a POSS species that phase-separated into crystallites (cyclohexyl-POSS), and two types of POSS that dispersed on a molecular scale in the PMMA (methacryl-POSS and trisilanol-phenyl-POSS). All three of these types of POSS, when incorporated separately, toughen PMMA at low loadings (≤ 5 wt%) in slow-speed tension. However, all of these binary blends are highly flaw sensitive and thus the reproducibility of the toughening is poor. The combined addition of the crystallizable cyclohexyl-POSS and the molecularly-dispersed methacryl-POSS leads to not only the highest toughness values (an increase by a factor of 4 over PMMA) but also excellent reproducibility of the toughening, while not sacrificing the modulus. The reproducible toughening observed in the blends of cyclohexyl-POSS, methacryl-POSS, and PMMA is due to the large amount of plastic deformation required to form the distinct crack structure in these ternary blends, which leads to reduced flaw sensitivity.

Acknowledgements

This research was sponsored by the DURINT program of the US Air Force under grant F49620-01-1-0447. Special thanks are given to Darrell Marchant, Tim Haddad, and Pat Ruth at Edwards Air Force Base for help in setting up experiments and for helpful discussions.

References

[1] Brown HR, Argon AS, Cohen RE, Gebizlioglu OS, Kramer EJ. Macromolecules 1989;22:1002.
[2] Cho K, Yang J, Kang BI, Park CE. J Appl Polym Sci 2003;89:3115.
[3] Cho K, Yang J, Yoon S, Hwang M, Nair SV. J Appl Polym Sci 2005;95:748.
[4] Ash BJ, Siegel RW, Schadler LS. Macromolecules 2004;37:1358.
[5] Argon AS. J Appl Polym Sci 1999;72:13.
[6] Piorkowska E, Argon AS, Cohen RE. Polymer 1993;34:4435.
[7] Qin J, Argon AS, Cohen RE. J Appl Polym Sci 1999;71:2319.
[8] Jansen BJP, Rastogi S, Meijer HEH, Lemstra PJ. Macromolecules 2001;34:3998.
[9] Gorga RE, Cohen RE. J Polym Sci, Part B: Polym Phys 2004;42:2690.
[10] Gilbert DG, Donald AM. J Mater Sci 1986;21:1819.
[11] Bartczak Z, Argon AS, Cohen RE, Weinberg M. Polymer 1999;40:2347.
[12] Thio YS, Cohen RE, Argon AS, Weinberg M. Polymer 2002;43:3661.
[13] Kopesky ET, Haddad TS, Cohen RE, McKinley GH. Macromolecules 2004;37:8992.
[14] Kopesky ET, Haddad TS, Cohen RE, McKinley GH. Polymer 2005;46:4743.
[15] Mulliken AD, Boyce MC. J Int Solids Struct, in press.
[16] Davies E. Philos Trans, A 1948;240:375.
[17] Kolsky H. Proc Phys Soc, B 1949;62:676.
[18] Gray G. in ASM handbook 2000;462–76.
[19] Wilbrink MWL, Argon AS, Cohen RE, Weinberg M. Polymer 2001;42:10155.